

Analytic explanation of spatial resolution related to bandwidth and detector aperture size in thermoacoustic or photoacoustic reconstruction

Minghua Xu and Lihong V. Wang*

Optical Imaging Laboratory, Department of Biomedical Engineering, Texas A&M University, 3120 TAMU, College Station, Texas 77843-3120

(Received 31 October 2002; published 9 May 2003)

An analytic explanation of the spatial resolution in thermoacoustic or photoacoustic reconstruction is presented. Three types of specific recording geometries, including spherical, planar, and cylindrical surface, as well as other general cases, are investigated. Analytic expressions of the point-spread functions (PSF's), as a function of the bandwidth of the measurement system and the finite size of the detector aperture, are derived based on rigorous reconstruction formulas. The analyses clearly reveal that the dependence of the PSF's on the bandwidth of all recording geometries shares the same space-invariant expression while the dependence on the aperture size of the detector differs. The bandwidth affects both axial and lateral resolutions; in contrast, the detector aperture blurs the lateral resolution greatly but the axial resolution only slightly.

DOI: 10.1103/PhysRevE.67.056605

PACS number(s): 43.35.+d, 87.57.Ce, 43.60.+d, 43.80.+p

I. INTRODUCTION

In the last decade, thermoacoustic or photoacoustic tomography of soft tissue utilizing excitation from a pulsed electromagnetic (EM) energy source, such as radio frequency or laser, has attracted considerable attention [1–12]. With this technique, it is assumed that, following a short pulse of EM illumination, a spatial distribution of acoustic pressure inside the tissue is simultaneously excited by thermoelastic expansion, which acts as a source for acoustic response. The intensity of the acoustic pressure is strongly related to the locally absorbed EM energy. A wide range of EM absorption coefficients in soft tissue contributes to a good contrast between different types of tissues. The effect of thermal diffusion on thermoacoustic or photoacoustic waves in tissue is always ignored, since the EM pulse duration is often so short that the thermal conduction time is far greater than the acoustic transit time through the heterogeneities of the EM energy depositions. The acoustic waves from the initial acoustic source propagate toward the surface of the tissues with various time delays. Ultrasound detectors are placed around the tissue to record the outgoing acoustic waves, referred to as the thermoacoustic or photoacoustic signals, which carry information about EM absorption as well as about the acoustic properties of the tissue. For medical imaging and diagnostics, an appropriate reconstruction algorithm is required to map the initial acoustic sources, or EM absorption distribution.

To detect thermoacoustic signals, one approach is to use focused ultrasound transducers, in which the lateral resolution is determined by the focal diameter of the transducer and the axial resolution by the bandwidth [5,6]. Another approach is to use small-aperture unfocused detectors—ideally, point detectors—that can receive ultrasound from a large

angle of acceptance. Thus far, rigorous reconstruction algorithms have been reported with point-detector measurements from idealized recording configurations, including the fully enclosing spherical recording surface [7], the planar recording surface of an infinite extent [3,8], and the cylindrical recording surface of an infinite length [9]. In these algorithms, the acoustic property of the tissue is often assumed to be homogenous as the speed of sound in soft tissue is relatively constant at ~ 1.5 mm/ μ s. Details can be found in Ref. [7] of the reconstruction formulas for spherical geometry and in Refs. [8,9,11] for the planar and cylindrical geometries.

Spatial resolution is one of the most important parameters in thermoacoustic reconstruction. Acoustic inhomogeneity blurs the reconstructed image, but in some cases, the blurring can be corrected. A limited view also affects spatial resolution due to lack of sufficient data; in this case, the reconstruction is incomplete and reconstruction artifacts occur [12]. These two topics will not be addressed in this paper. There are two other main factors that limit spatial resolution—the finite bandwidth of the detection system and the size of the detector aperture. Past research work has only estimated the spatial resolution in thermoacoustic tomography based on measurements or numerical simulations. No theoretical analysis has been reported.

In this paper, a complete theoretical explanation of the degree of spatial resolution that results from varying the bandwidth as well as the detector aperture will be presented. Analytic expressions of point-spread functions (PSF's) on the spherical, planar, and cylindrical recording surfaces will be explicitly derived. The paper is organized as follows. In Sec. II, the inverse problem and the reconstruction formulas for thermoacoustic tomography will be briefly reviewed. Detailed derivations of bandwidth-limited PSF's in the above three measurement geometries as well as more general cases will be presented in Secs. III A, III B, III C, and III D, respectively; and resolution will be discussed in Sec. III E. In Sec. IV, detailed derivations of PSF's as a function of detector aperture size will be shown in Secs. IV A, IV B, and IV C. Section V will provide discussion and conclusions.

*Author to whom all correspondence should be addressed. FAX: 979-845-4450; electronic address: LWang@tamu.edu; URL: <http://oilab.tamu.edu>

II. RECONSTRUCTION FORMULAS

We will first briefly review the inverse problem and the rigorous reconstruction formulas for thermoacoustic tomography. It is well known that, in response to a heat source, the pressure $p(\mathbf{r}, t)$ at position \mathbf{r} and time t in an acoustically homogeneous medium obeys the following equation [13]:

$$\nabla^2 p(\mathbf{r}, t) - \frac{1}{c^2} \frac{\partial^2 p(\mathbf{r}, t)}{\partial t^2} = -\frac{\beta}{C_p} \frac{\partial H(\mathbf{r}, t)}{\partial t}, \quad (1)$$

where C_p is the specific heat, $H(\mathbf{r}, t)$ is the heating function defined as the thermal energy deposited by the EM radiation per time and volume, β is the isobaric volume expansion coefficient, and c is the speed of sound. The heating function can be written as the product of a spatial absorption function and a temporal illumination function:

$$H(\mathbf{r}, t) = A(\mathbf{r})I(t). \quad (2)$$

Assuming that the illumination is a Dirac δ function such as $I(t) = \delta(t)$, and taking the following Fourier transform on variable $\bar{t} = ct$,

$$\tilde{p}(\mathbf{r}, k) = \int_{-\infty}^{+\infty} p(\mathbf{r}, \bar{t}) \exp(ik\bar{t}) d\bar{t}, \quad (3)$$

the solution of Eq. (1) becomes the integral

$$\tilde{p}(\mathbf{r}_0, k) = -ikc^2 \eta \int \int \int_V d^3r A(\mathbf{r}) \tilde{G}_k(\mathbf{r}, \mathbf{r}_0), \quad (4)$$

where $\eta = \beta/C_p$ and $\tilde{G}_k(\mathbf{r}, \mathbf{r}_0)$ is the Green's function satisfying the following equation:

$$(\nabla^2 + k^2) \tilde{G}_k(\mathbf{r}, \mathbf{r}_0) = -\delta(\mathbf{r} - \mathbf{r}_0). \quad (5)$$

In general, the Green's function in three-dimensional free space can be written as [14]

$$\tilde{G}_k(\mathbf{r}, \mathbf{r}_0) = \frac{\exp(ik|\mathbf{r} - \mathbf{r}_0|)}{4\pi|\mathbf{r} - \mathbf{r}_0|}. \quad (6)$$

Actually, the initial thermoacoustic pressure excited by the $\delta(t)$ EM illumination is equal to $p_0(\mathbf{r}) = \Gamma(\mathbf{r})A(\mathbf{r})$, where the Grüneisen parameter $\Gamma(\mathbf{r}) = \eta(\mathbf{r})c^2$ may be inhomogeneous. Then, Eq. (4) can be expressed by the following form:

$$\tilde{p}(\mathbf{r}_0, k) = -ik \int \int \int_V d^3r \tilde{G}_k(\mathbf{r}, \mathbf{r}_0) p_0(\mathbf{r}). \quad (7)$$

The inverse problem is to reconstruct the absorption distribution $A(\mathbf{r})$ or the initial thermoacoustic pressure distribution $p_0(\mathbf{r})$ from a set of data $p(\mathbf{r}_0, t)$ or $\tilde{p}(\mathbf{r}_0, k)$ measured at position \mathbf{r}_0 . In general, the Green's function can be expanded in terms of some appropriate functions for the corre-

sponding recording geometries. Then, based on the orthogonality of the appropriate functions, reconstruction formulas can be derived.

In spherical recording geometry, it is assumed that the recording surface is a spherical surface $\mathbf{r}_0 = (r_0, \theta_0, \varphi_0)$ in the spherical polar coordinates $\mathbf{r} = (r, \theta, \varphi)$, where θ is the polar angle from the z axis and φ is the azimuthal angle in the x - y plane from the x axis. The sample under study lies inside the sphere, i.e., $A(\mathbf{r}) = A(r, \theta, \varphi)$ where $r < r_0$ and $A(\mathbf{r}) = 0$ when $r > r_0$. The rigorous reconstruction formula for $A(\mathbf{r})$ can be written as [7]

$$A(\mathbf{r}) = \frac{1}{2\pi^2 c^2 \eta} \int \int_{\Omega_0} d\Omega_0 \int_0^{+\infty} dk \tilde{p}(\mathbf{r}_0, k) \times \sum_{m=0}^{\infty} \frac{(2m+1)j_m(kr)}{h_m^{(1)}(kr_0)} P_m(\mathbf{n}_0 \cdot \mathbf{n}), \quad (8)$$

where $d\Omega_0 = \sin \theta_0 d\theta_0 d\varphi_0$; $\mathbf{n} = \mathbf{r}/r$ and $\mathbf{n}_0 = \mathbf{r}_0/r_0$ are unit vectors; $j_m(\cdot)$, $h_m^{(1)}(\cdot)$, and $P_m(\cdot)$ are the spherical Bessel function of the first kind, the spherical Hankel function of the first kind, and the Legendre polynomial function, respectively. In addition, the integral range over variable k in Eq. (8) can extend to from $-\infty$ to 0 by simply taking the complex conjugate and using the following properties: $\tilde{p}^*(\mathbf{r}_0, k) = \tilde{p}(\mathbf{r}_0, -k)$, $[j_n(z)]^* = j_n(z)$, and $[h_n^{(1)}(z)]^* = h_n^{(2)}(z)$ when z is real and positive, where “ $*$ ” stands for the complex conjugate.

In planar recording geometry, it is assumed that the measurement surface is the $z=0$ plane, i.e., $\mathbf{r}_0 = (x_0, y_0, 0)$ in the Cartesian coordinates $\mathbf{r} = (x, y, z)$. The sample lies above the plane, i.e., $A(\mathbf{r}) = A(x, y, z)$ where $z > 0$ and $A(\mathbf{r}) = 0$ when $z < 0$. The rigorous reconstruction formula for $A(\mathbf{r})$ can be written as [8,11]

$$A(x, y, z) = \frac{1}{4\pi^3 c^2 \eta} \int \int_{-\infty}^{+\infty} dx_0 dy_0 \int_{-\infty}^{+\infty} dk \tilde{p}(\mathbf{r}_0, k) \times \int \int_{\rho=0}^{\rho=|k|} du dv \times \exp[-iz \operatorname{sgn}(k) \sqrt{k^2 - \rho^2}] \exp[iu(x_0 - x) + iv(y_0 - y)], \quad (9)$$

where $\rho = \sqrt{u^2 + v^2}$, $\operatorname{sgn}(k) = 1$ when $k > 0$, and $\operatorname{sgn}(k) = -1$ when $k < 0$.

In cylindrical recording geometry, it is assumed that the measurement surface is a circular cylindrical surface $\mathbf{r}_0 = (\rho_0, \varphi_0, z_0)$ in the circular cylindrical coordinates $\mathbf{r} = (\rho, \varphi, z)$. The sample lies in the cylinder, i.e., $A(\mathbf{r}) = A(\rho, \varphi, z)$ when $\rho < \rho_0$, and $A(\mathbf{r}) = 0$ when $\rho > \rho_0$. The rigorous reconstruction formula for $A(\mathbf{r})$ can be written as [9,11]

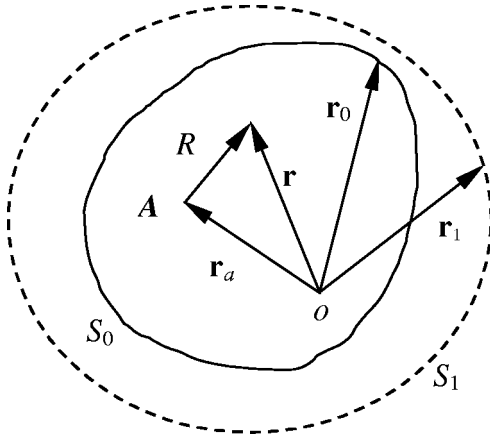


FIG. 1. Diagram of the recording geometry: a recording surface S_1 completely encloses another recording surface S_0 ; there is a point source A at \mathbf{r}_a inside S_0 ; R is the distance between an arbitrary point at \mathbf{r} and the point source A ; \mathbf{r}_0 and \mathbf{r}_1 point to a detection element on the surfaces S_0 and S_1 , respectively.

$$\begin{aligned}
 A(\rho, \varphi, z) &= \frac{1}{2\pi^3 c^2 \eta} \int_0^{2\pi} d\varphi_0 \int_{-\infty}^{+\infty} dz_0 \int_0^{+\infty} dk \tilde{p}(\mathbf{r}_0, k) \\
 &\times \int_{-k}^{+k} d\gamma \exp[i\gamma(z_0 - z)] \\
 &\times \sum_{n=-\infty}^{+\infty} \exp[in(\varphi_0 - \varphi)] \frac{J_n(\rho\sqrt{k^2 - \gamma^2})}{H_n^{(1)}(\rho_0\sqrt{k^2 - \gamma^2})}, \quad (10)
 \end{aligned}$$

where $J_n(\cdot)$ and $H_n^{(1)}(\cdot)$ are the Bessel function of the first kind and the Hankel function of the first kind, respectively. In addition, the integral range over variable k in Eq. (10) can extend to from $-\infty$ to 0 , by simply taking the complex conjugate and using the following properties: $\tilde{p}^*(\mathbf{r}_0, k) = \tilde{p}(\mathbf{r}_0, -k)$, $[J_n(z)]^* = J_n(z)$, and $[H_n^{(1)}(z)]^* = H_n^{(2)}(z)$ when z is real and positive.

III. BANDWIDTH-LIMITED PSF

As shown in Fig. 1, assuming a point source $A(\mathbf{r}) = \delta(\mathbf{r} - \mathbf{r}_a)$ at \mathbf{r}_a , the pressure at the recording point \mathbf{r}_0 can be expressed as

$$\tilde{p}(\mathbf{r}_0, k) = -ikc^2 \eta \tilde{G}_k(\mathbf{r}_a, \mathbf{r}_0). \quad (11)$$

Suppose the detection system is bandlimited in the temporal-frequency domain and characterized by a low-pass function $\tilde{H}(k)$. The amplitude of the acoustic wave vector $k = \omega/c$, where ω is the acoustic angular frequency. The detected signal at the recording surface \mathbf{r}_0 becomes $\tilde{p}'(\mathbf{r}_0, k) = \tilde{H}(k)\tilde{p}(\mathbf{r}_0, k)$ instead of $\tilde{p}(\mathbf{r}_0, k)$. But the reconstruction formulas, Eqs. (8)–(10), for point-detector measurements in the spherical, planar, and cylindrical recording geometries, respectively, remain the same. Replacing $\tilde{p}(\mathbf{r}_0, k)$ by $\tilde{p}'(\mathbf{r}_0, k)$ in these reconstruction formulas will give us the

bandwidth-limited analytic expressions of the PSF's to be derived below for the different geometries.

A. Spherical geometry

The point source at $\mathbf{r}_a = (r_a, \theta_a, \varphi_a)$ in the spherical coordinates can be written as

$$A(\mathbf{r}) = \frac{1}{r^2} \delta(r - r_a) \delta(\varphi - \varphi_a) \delta(\cos \theta - \cos \theta_a). \quad (12)$$

The Green's function can be expanded according to the following identity ($r_0 > r_a, k > 0$) [14]:

$$\tilde{G}_k(\mathbf{r}_a, \mathbf{r}_0) = \frac{ik}{4\pi} \sum_{l=0}^{\infty} (2l+1) j_l(kr_a) h_l^{(1)}(kr_0) P_l(\mathbf{n}_a \cdot \mathbf{n}_0), \quad (13)$$

where $\mathbf{n}_a = \mathbf{r}_a/r_a$.

Replacing $\tilde{p}(\mathbf{r}_0, k)$ by $\tilde{p}'(\mathbf{r}_0, k)$ in Eq. (8) and considering the following identity [14]:

$$\int \int_{\Omega_0} d\Omega_0 P_l(\mathbf{n}_a \cdot \mathbf{n}_0) P_m(\mathbf{n}_0 \cdot \mathbf{n}) = \frac{4\pi}{2l+1} \delta_{lm} P_l(\mathbf{n}_a \cdot \mathbf{n}), \quad (14)$$

the resulting reconstruction for $A(\mathbf{r})$ is

$$\begin{aligned}
 A_b(\mathbf{r}) &= \frac{1}{2\pi^2} \int_0^{+\infty} \tilde{H}(k) k^2 dk \sum_{m=0}^{\infty} (2m+1) \\
 &\times P_m(\mathbf{n}_a \cdot \mathbf{n}) j_m(kr_a) j_m(kr). \quad (15)
 \end{aligned}$$

Further, taking into account the following identity [15]:

$$\sum_{m=0}^{\infty} (2m+1) P_m(\mathbf{n}_a \cdot \mathbf{n}) j_m(kr_a) j_m(kr) = \frac{\sin(kR)}{kR} = j_0(kR), \quad (16)$$

where $R = \sqrt{r_a^2 + r^2 - 2r_a r \cos(\mathbf{n}_a \cdot \mathbf{n})}$, one can obtain

$$A_b(\mathbf{r}) = \frac{1}{2\pi^2} \int_0^{+\infty} \tilde{H}(k) j_0(kR) k^2 dk. \quad (17)$$

Particularly, if $\tilde{H}(k) \equiv 1$ for $k = 0 \rightarrow \infty$, considering the following identities [14]:

$$\int_0^{+\infty} j_m(kr) j_m(kr_a) k^2 dk = \frac{\pi}{2r^2} \delta(r - r_a), \quad (18)$$

$$\sum_{m=0}^{\infty} (2m+1) P_m(\mathbf{n}_a \cdot \mathbf{n}) = 4\pi \delta(\varphi - \varphi_a) \delta(\cos \theta - \cos \theta_a), \quad (19)$$

Eq. (15) reduces to a point source the same as the expression in Eq. (12), which actually verifies the reconstruction Eq. (8).

B. Planar geometry

The point source at $\mathbf{r}_a = (x_a, y_a, z_a)$ in the Cartesian coordinates can be written as

$$A(x, y, z) = \delta(x - x_a) \delta(y - y_a) \delta(z - z_a). \quad (20)$$

The Green's function can be expanded as [14]

$$\tilde{G}_k(\mathbf{r}_a, \mathbf{r}_0) = \frac{1}{(2\pi)^3} \int \int \int_{-\infty}^{+\infty} d^3K \frac{\exp[i\mathbf{K} \cdot (\mathbf{r}_0 - \mathbf{r}_a)]}{K^2 - k^2}, \quad (21)$$

where $\mathbf{K} = (K_x, K_y, K_z)$.

Using the detected signal at the recording surface \mathbf{r}_0 , $\tilde{p}'(\mathbf{r}_0, k) = \tilde{H}(k) \tilde{p}(\mathbf{r}_0, k)$, to replace $\tilde{p}(\mathbf{r}_0, k)$ in the reconstruction Eq. (9), and considering the following identities:

$$\int_{-\infty}^{+\infty} \exp[i(u + K_x)x_0] dx_0 = 2\pi \delta(K_x + u), \quad (22)$$

$$\int_{-\infty}^{+\infty} \exp[i(v + K_y)y_0] dy_0 = 2\pi \delta(K_y + v), \quad (23)$$

$$\begin{aligned} & \int_{-\infty}^{+\infty} dK_z \frac{\exp(-iK_z z_a)}{K_z^2 + \rho^2 - k^2} \\ &= i\pi \operatorname{sgn}(k) \frac{\exp[iz_a \operatorname{sgn}(k) \sqrt{k^2 - \rho^2}]}{\sqrt{k^2 - \rho^2}}, \quad |k| > \rho, \end{aligned} \quad (24)$$

the resulting reconstruction for $A(\mathbf{r})$ is

$$\begin{aligned} A_b(x, y, z) &= \frac{1}{(2\pi)^3} \int_{-\infty}^{+\infty} k dk \tilde{H}(k) \int \int_{\rho=0}^{\rho=|k|} du dv \\ & \times \exp(-iu\Delta x - iv\Delta y) \\ & \times \operatorname{sgn}(k) \frac{\exp[-i \operatorname{sgn}(k) \Delta z \sqrt{k^2 - \rho^2}]}{\sqrt{k^2 - \rho^2}}, \end{aligned} \quad (25)$$

where $\Delta x = x - x_a$, $\Delta y = y - y_a$, and $\Delta z = z - z_a$.

In the evaluation of the integral in Eq. (24), we replaced k with $k + i\gamma$ as suggested in Ref. [14], where γ is a small positive real number. Since there will be some damping of the wave in a physical system, we then complete a contour integral in the complex plane and let γ approach zero.

Changing the integration order of $du dv$ and dk , and further letting $w = \operatorname{sgn}(k) \sqrt{k^2 - \rho^2}$, Eq. (25) reduces to

$$\begin{aligned} A_b(x, y, z) &= \frac{1}{(2\pi)^3} \int \int \int_{-\infty}^{+\infty} du dv dw \\ & \times \exp(-iu\Delta x - iv\Delta y - iw\Delta z) \tilde{H}(k), \end{aligned} \quad (26)$$

where $k^2 = u^2 + v^2 + w^2$.

Particularly, if $\tilde{H}(k) \equiv 1$ for $-\infty < k < \infty$, Eq. (26) becomes a point source as the original one in Eq. (20).

In general, by changing the integral from the Cartesian coordinates into the spherical coordinates,

$$(u, v, w) \rightarrow \mathbf{k} = (k, \theta, \varphi),$$

$$(\Delta x, \Delta y, \Delta z) \rightarrow \mathbf{R} = (R, \alpha, \beta),$$

where $R^2 = (\Delta x)^2 + (\Delta y)^2 + (\Delta z)^2$, one can rewrite Eq. (26) as

$$A_b(x, y, z) = \frac{1}{(2\pi)^3} \int \int \int \exp(-i\mathbf{k} \cdot \mathbf{R}) \tilde{H}(k) d^3\mathbf{k}. \quad (27)$$

The integration of Eq. (27) can be further simplified to

$$\begin{aligned} A_b(x, y, z) &= \frac{1}{(2\pi)^3} \int_0^{+\infty} \tilde{H}(k) k^2 dk \\ & \times \int_0^\pi \exp(-ikR \cos \gamma) \sin \gamma d\gamma 2\pi, \end{aligned} \quad (28)$$

where γ is the angle between \mathbf{k} and \mathbf{R} , i.e.,

$$A_b(x, y, z) = \frac{1}{2\pi^2} \int_0^{+\infty} \tilde{H}(k) j_0(kR) k^2 dk. \quad (29)$$

C. Cylindrical geometry

The point source at $\mathbf{r}_a = (\rho_a, \varphi_a, z_a)$ in the cylindrical coordinates can be written as

$$\begin{aligned} A(\rho, \varphi, z) &= \frac{1}{\rho} \delta(\rho - \rho_a) \delta(\varphi - \varphi_a) \delta(z - z_a) \\ &= \frac{1}{\rho} \delta(\rho - \rho_a) \frac{1}{2\pi} \sum_{m=-\infty}^{+\infty} \exp[im(\varphi - \varphi_a)] \\ & \times \frac{1}{2\pi} \int_{-\infty}^{+\infty} \exp[ik_z(z - z_a)] dk_z. \end{aligned} \quad (30)$$

The Green's function can be expanded as ($k > 0$) [11,14,17]

$$\begin{aligned} \tilde{G}_k(\mathbf{r}_a, \mathbf{r}_0) &= \frac{i}{8\pi} \sum_{m=-\infty}^{+\infty} \exp[im(\varphi_a - \varphi_0)] \\ & \times \int_{-\infty}^{+\infty} dk_z \exp[ik_z(z_a - z_0)] \\ & \times J_m(\mu\rho_a) H_m^{(1)}(\mu\rho_0), \end{aligned} \quad (31)$$

where $\mu = \sqrt{k^2 - k_z^2}$ when $k_z^2 < k^2$, and $\mu = i\sqrt{k_z^2 - k^2}$ when $k_z^2 > k^2$.

Using the detected signal at the recording surface \mathbf{r}_0 , $\tilde{p}'(\mathbf{r}_0, k) = \tilde{H}(k) \tilde{p}(\mathbf{r}_0, k)$ to replace $\tilde{p}(\mathbf{r}_0, k)$ in the reconstruction Eq. (10), and considering the following identities:

$$\int_0^{2\pi} d\varphi_0 \exp[i\varphi_0(n-m)] = 2\pi\delta_{nm}, \quad (32)$$

$$\int_{-\infty}^{+\infty} dz_0 \exp[iz_0(\gamma-k_z)] = 2\pi\delta(\gamma-k_z), \quad (33)$$

the resulting reconstruction for $A(\mathbf{r})$ is

$$A_b(\rho, \varphi, z) = \frac{1}{4\pi^2} \int_0^{+\infty} k dk \tilde{H}(k) \int_{-k}^{+k} dk_z \exp[ik_z(z_a - z)] \\ \times \sum_{m=-\infty}^{+\infty} \exp[im(\varphi_a - \varphi)] J_m(\mu\rho_a) J_m(\mu\rho). \quad (34)$$

Changing the integration order of variables k and k_z and taking into account the following identity [15]:

$$\sum_{m=-\infty}^{+\infty} \exp[im(\varphi_a - \varphi)] J_m(\mu\rho_a) J_m(\mu\rho) = J_0(\mu D), \quad (35)$$

where $D = \sqrt{\rho_a^2 + \rho^2 - 2\rho_a\rho \cos(\varphi_a - \varphi)}$, one can simplify Eq. (34) to

$$A_b(\rho, \varphi, z) = \frac{1}{4\pi^2} \int_{-\infty}^{+\infty} dk_z \exp[ik_z(z_a - z)] \\ \times \int_{|k_z|}^{+\infty} k \tilde{H}(k) dk J_0(\mu D). \quad (36)$$

By changing the integral variable k with $\mu = \sqrt{k^2 - k_z^2}$, one can get

$$A_b(\rho, \varphi, z) = \frac{1}{4\pi^2} \int_{-\infty}^{+\infty} dk_z \exp[-ik_z\Delta z] \\ \times \int_0^{+\infty} \tilde{H}(k) \mu d\mu J_0(\mu D), \quad (37)$$

where $k^2 = k_z^2 + \mu^2$, $\Delta z = z - z_a$.

Then, one can denote $\Delta x = x - x_a = D \cos \beta$ and $\Delta y = y - y_a = D \sin \beta$, and introduce $k_x = \mu \cos \alpha$ and $k_y = \mu \sin \alpha$, where $D = \sqrt{(\Delta x)^2 + (\Delta y)^2}$ and $\mu = \sqrt{k_x^2 + k_y^2}$, and rewrite the far right integral in Eq. (37) as

$$\int_0^{+\infty} \mu d\mu H(k) J_0(\mu D) = \frac{1}{2\pi} \int \int_{-\infty}^{+\infty} dk_x dk_y \\ \times \exp(-ik_x\Delta x - ik_y\Delta y) \tilde{H}(k), \quad (38)$$

where $k^2 = k_z^2 + \mu^2 = k_x^2 + k_y^2 + k_z^2$.

Therefore, Eq. (37) can be rewritten as

$$A_b(\rho, \varphi, z) = \frac{1}{(2\pi)^3} \int \int \int_{-\infty}^{+\infty} dk_z dz_x dk_y \tilde{H}(k) \\ \times \exp(-ik_x\Delta x - ik_z\Delta y - ik_z\Delta z), \quad (39)$$

which is the same as Eq. (26). Thus, $A_b(\rho, \varphi, z)$ takes the same form as Eq. (29),

$$A_b(\rho, \varphi, z) = \frac{1}{2\pi^2} \int_0^{+\infty} \tilde{H}(k) j_0(kR) k^2 dk, \quad (40)$$

where

$$R = \sqrt{(\Delta x)^2 + (\Delta y)^2 + (\Delta z)^2} \\ = \sqrt{\rho_a^2 + \rho^2 - 2\rho_a\rho \cos(\varphi_a - \varphi) + (\Delta z)^2}.$$

Particularly, if $\tilde{H}(k) \equiv 1$ for $k=0 \rightarrow \infty$, Eq. (39) reduces to a point source the same as the original one.

D. General geometry

We have proved that the bandwidth-limited PSF's in the three different geometries share the same expression as shown in Eqs. (17), (29), and (40). As described in these equations, the PSF is independent of the position of the point source but dependent on the distance R from the point source. Therefore, the PSF due to bandwidth is space invariant.

Actually, the space invariance of PSF due to bandwidth can be extended to more general recording geometries. As mentioned in Ref. [11], the reconstruction for $A(\mathbf{r})$ can be expressed by a linear integral:

$$A(\mathbf{r}) = \int \int_{S_0} dS_0 \int_k dk \tilde{K}_k(\mathbf{r}_0, \mathbf{r}) \tilde{p}(\mathbf{r}_0, k), \quad (41)$$

where S_0 is the recording surface, which covers the object under study.

The inverse problem for thermoacoustic reconstruction is to seek such an integral kernel $\tilde{K}_k(\mathbf{r}_0, \mathbf{r})$ for a particular recording surface. For the spherical, planar, and cylindrical recording geometries, the integral kernel $\tilde{K}_k(\mathbf{r}_0, \mathbf{r})$ can be explicitly given as shown in Eqs. (8), (9), and (10), respectively. For other recording geometries, the integral kernel $\tilde{K}_k(\mathbf{r}_0, \mathbf{r})$ is more complicated or even nonexistent analytically.

As shown in Fig. 1, suppose another recording surface S_1 , which could be a spherical, planar, or cylindrical recording surface, can completely enclose surface S_0 . Then, based on Green's theorem [17], the pressure $\tilde{p}(\mathbf{r}_1, k)$ at S_1 can be computed by the pressure $\tilde{p}(\mathbf{r}_0, k)$ on surface S_0 ,

$$\tilde{p}(\mathbf{r}_1, k) = \int \int_{S_0} dS_0 \left(\tilde{p}(\mathbf{r}_0, k) \frac{\partial \tilde{G}_k(\mathbf{r}_1, \mathbf{r}_0)}{\partial n_0^s} \right. \\ \left. - \tilde{G}_k(\mathbf{r}_1, \mathbf{r}_0) \frac{\partial \tilde{p}(\mathbf{r}_0, k)}{\partial n_0^s} \right), \quad (42)$$

where $\partial/\partial n_0^s$ is the normal component of the gradient on surface S_0 and points outward away from the acoustic source; and \mathbf{r}_0 and \mathbf{r}_1 represent detection positions on surfaces S_0 and S_1 , respectively. Since the reconstruction based on Eq. (41) from the measurement on surface S_0 is exact, the pressure $\tilde{p}(\mathbf{r}_1, k)$ on surface S_1 must be identical to the thermoacoustic pressure directly generated by the source $A(\mathbf{r})$:

$$\tilde{p}(\mathbf{r}_1, k) = \int \int \int_{V_0} dV_0 A(\mathbf{r}) \tilde{G}_k(\mathbf{r}_1, \mathbf{r}), \quad (43)$$

where V_0 is the volume enclosed by S_0 .

Now, considering the bandwidth characterized by $\tilde{H}(k)$, one can rewrite the reconstruction Eq. (41) as

$$A_b(\mathbf{r}) = \int \int_{S_0} dS_0 \int_{-\infty}^{+\infty} dk \tilde{K}_k(\mathbf{r}_0, \mathbf{r}) [\tilde{H}(k) \tilde{p}(\mathbf{r}_0, k)]. \quad (44)$$

In other words, Eq. (44) gives the exact reconstruction of a new and unique source $A_b(\mathbf{r})$ from $\tilde{H}(k) \tilde{p}(\mathbf{r}_0, k)$ measured on surface S_0 :

$$\tilde{H}(k) \tilde{p}(\mathbf{r}_0, k) = \int \int \int_{V_0} dV_0 A_b(\mathbf{r}) \tilde{G}_k(\mathbf{r}_0, \mathbf{r}). \quad (45)$$

Based on Green's theorem, the pressure on surface S_1 can be computed by the pressure $\tilde{H}(k) \tilde{p}(\mathbf{r}_0, k)$ on surface S_0 , which is found equal to $\tilde{H}(k) \tilde{p}(\mathbf{r}_1, k)$ with considering Eq. (42):

$$\begin{aligned} & \int \int_{S_0} dS_0 \left([\tilde{H}(k) \tilde{p}(\mathbf{r}_0, k)] \frac{\partial \tilde{G}_k(\mathbf{r}_1, \mathbf{r}_0)}{\partial n_0^s} \right. \\ & \quad \left. - \tilde{G}_k(\mathbf{r}_1, \mathbf{r}_0) \frac{\partial [\tilde{H}(k) \tilde{p}(\mathbf{r}_0, k)]}{\partial n_0^s} \right) \\ & = \tilde{H}(k) \int \int_{S_0} dS_0 \left(\tilde{p}(\mathbf{r}_0, k) \frac{\partial \tilde{G}_k(\mathbf{r}_1, \mathbf{r}_0)}{\partial n_0^s} \right. \\ & \quad \left. - \tilde{G}_k(\mathbf{r}_1, \mathbf{r}_0) \frac{\partial \tilde{p}(\mathbf{r}_0, k)}{\partial n_0^s} \right) \\ & = \tilde{H}(k) \tilde{p}(\mathbf{r}_1, k). \end{aligned} \quad (46)$$

This pressure must be identical to the thermoacoustic pressure directly generated by the new source $A_b(\mathbf{r})$ in volume V_0 ,

$$\int \int \int_{V_0} dV_0 A_b(\mathbf{r}) \tilde{G}_k(\mathbf{r}_1, \mathbf{r}) = \tilde{H}(k) \tilde{p}(\mathbf{r}_1, k), \quad (47)$$

i.e.,

$$\tilde{H}(k) \tilde{p}(\mathbf{r}_1, k) = \int \int \int_{V_1} dV_1 A_b(\mathbf{r}) \tilde{G}_k(\mathbf{r}_1, \mathbf{r}), \quad (48)$$

since there is no source in the volume between the surfaces S_0 and S_1 .

Equation (48) indicates that the new source $A_b(\mathbf{r})$ could be restored from the value $\tilde{H}(k) \tilde{p}(\mathbf{r}_1, k)$ on surface S_1 , if an exact reconstruction from data only on surface S_1 does exist. In other words, the reconstruction for $A(\mathbf{r})$ from the measurement with the bandwidth $\tilde{H}(k)$ on surface S_0 is identical to the reconstruction from the measurement with the same bandwidth $\tilde{H}(k)$ on surface S_1 that fully encloses S_0 . Fortunately, we have already obtained the exact reconstruction formulas from measurements on such a surface S_1 as the spherical, planar, or cylindrical recording geometries. Therefore, the PSF of the point source at \mathbf{r}_a as a function of bandwidth $\tilde{H}(k)$ from the measurement on surface S_0 is nothing but the same expression as Eqs. (17), (29), and (40) for the above three specific recording geometries, respectively.

E. Resolution

For convenience, we can denote the PSF symbolically as $\mathcal{F}_b^{\text{PSF}}$,

$$\mathcal{F}_b^{\text{PSF}}(R) = \frac{1}{2\pi^2} \int_0^{+\infty} \tilde{H}(k) j_0(kR) k^2 dk, \quad (49)$$

where the subscript b represents bandwidth, and $R = |\mathbf{r} - \mathbf{r}_a|$. Equation (49) can be rewritten in another form as

$$\mathcal{F}_b^{\text{PSF}}(R) = \frac{-1}{4\pi R} \left[\frac{dH(R)}{dR} + \frac{dH(-R)}{dR} \right], \quad (50)$$

if we let $H(-\bar{t}) = H(\bar{t})$ and define the following Fourier transform:

$$H(\bar{t}) = \frac{1}{2\pi} \int_{-\infty}^{+\infty} \tilde{H}(k) \exp(-ik\bar{t}) dk, \quad (51)$$

where $H(\bar{t})$ is the corresponding temporal signal of $\tilde{H}(k)$.

If $\tilde{H}(k)$ has a cutoff frequency k_c , $\tilde{H}(k) = 1$ when $k \leq k_c$, $\tilde{H}(k) = 0$ when $k > k_c$, the integral in Eq. (49) can be carried out,

$$\begin{aligned} \mathcal{F}_b^{\text{PSF}}(R) & = \frac{1}{2\pi^2} \int_0^{k_c} j_0(kR) k^2 dk \\ & = \frac{k_c}{2\pi^2 R^2} \left(\frac{\sin(k_c R)}{k_c R} - \cos(k_c R) \right), \end{aligned} \quad (52)$$

i.e.,

$$\mathcal{F}_b^{\text{PSF}}(R) = \frac{k_c^3}{2\pi^2} \frac{j_1(k_c R)}{k_c R} = \frac{k_c^3}{6\pi^2} \frac{3j_1(k_c R)}{k_c R}. \quad (53)$$

By normalizing the PSF of Eq. (53), one can get

$$\mathcal{F}_b^{\text{PSF}}(R) = \frac{3j_1(k_c R)}{k_c R}. \quad (54)$$

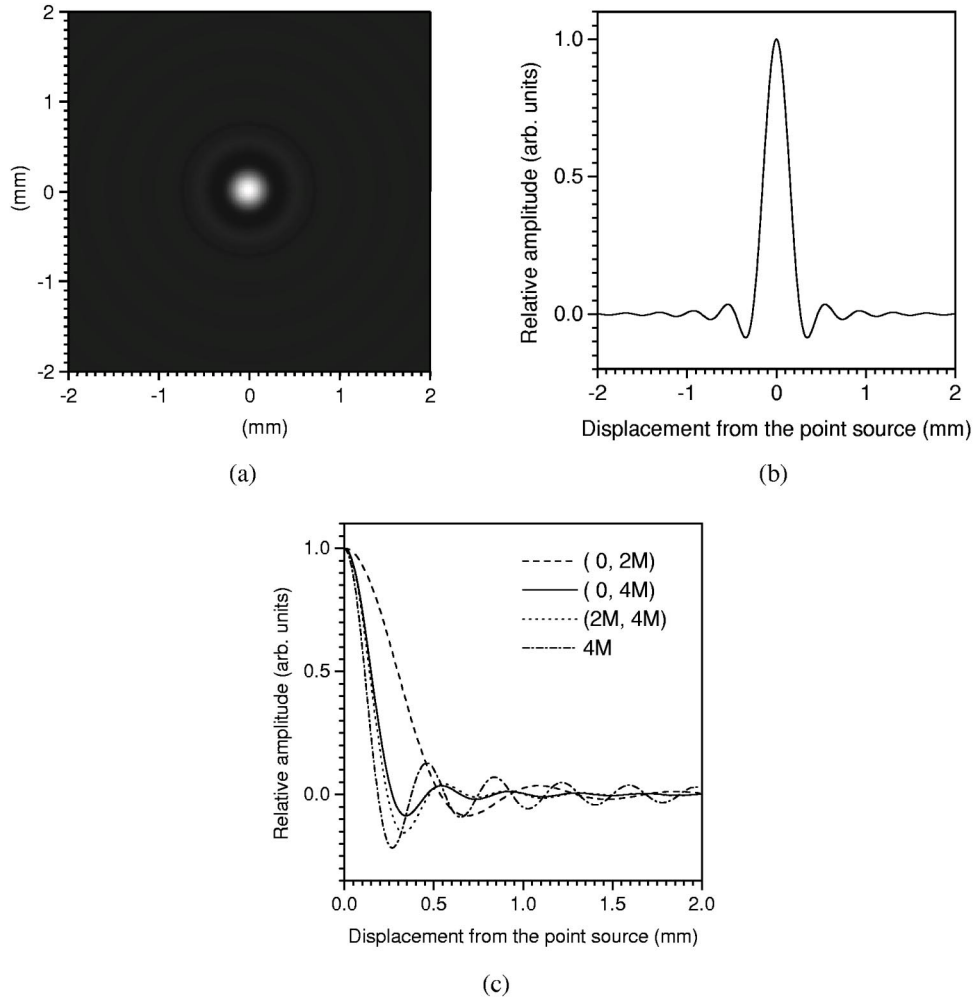


FIG. 2. An example of the PSF as a result of the bandwidth (0, 4 MHz): (a) a gray scale view and (b) a profile through the point source. (c) Comparison of the PSF's with different bandwidths: dashed line, (0, 2 MHz); solid line, (0, 4 MHz); dotted line, (2 MHz, 4 MHz); dot-dashed line, 4 MHz.

The full width at half maximum (FWHM) of the PSF is often used to represent the spatial resolution. It is easy to show $3j_1(x)/x = 0.5$ when $x = 2.4983$. Therefore,

$$\mathcal{W}_{\text{FWHM}} = 2 \times \frac{2.4983}{k_c} = 2 \times \frac{2.4983}{2\pi f_c/c} = 0.7952c/f_c \approx 0.8\lambda_c, \quad (55)$$

where λ_c is the wavelength at the cutoff frequency of the bandwidth. For example, if $c = 1.5 \text{ mm}/\mu\text{s}$, $f_c = 4 \text{ MHz}$, then $\mathcal{W}_{\text{FWHM}} \approx 0.3 \text{ mm}$. The corresponding $\mathcal{F}_b^{\text{PSF}}(R)$ is plotted in Figs. 2(a) and 2(b).

Sometimes, a detection system has a finite bandwidth characterized by a central frequency f_0 with a low cutoff frequency f_{Lc} and a high cutoff frequency f_{Hc} . For simplicity, suppose $\tilde{H}(k) = 1$ is in the above frequency range, and then the PSF can be expressed by

$$\mathcal{F}_b^{\text{PSF}}(R) = \frac{k_{\text{Hc}}^3}{2\pi^2} \frac{j_1(k_{\text{Hc}}R)}{k_{\text{Hc}}R} - \frac{k_{\text{Lc}}^3}{2\pi^2} \frac{j_1(k_{\text{Lc}}R)}{k_{\text{Lc}}R}, \quad (56)$$

where $k_{\text{Lc}} = 2\pi f_{\text{Lc}}/c$ and $k_{\text{Hc}} = 2\pi f_{\text{Hc}}/c$.

For example, a system is with $f_0 = 3 \text{ MHz}$, and $f_{\text{Lc}} = 2 \text{ MHz}$ and $f_{\text{Hc}} = 4 \text{ MHz}$. The corresponding PSF is plotted as the dotted line in Fig. 2(c). As shown in Fig. 2(c), the FWHM of the PSF with a bandwidth of (2 MHz, 4 MHz) is slightly narrower than the FWHM of the PSF with a wider bandwidth of (0, 4 MHz) [solid line in Fig. 2(c)]. In other words, due to the absence of a low frequency component, the high frequency component will cause the FWHM to be narrower. The minimum value of the FWHM can be estimated in the PSF with a single frequency f_c and zero bandwidth. The PSF in this case is nothing but the integral kernel in Eq. (49): the zero-order spherical Bessel function $j_0(k_c R)$. Such an example, with $f_c = 4 \text{ MHz}$, is plotted as the dash-dot line in Fig. 2(c). Since $j_0(1.895) \approx 0.5$, the minimum $\mathcal{W}_{\text{FWHM}} \approx 0.6\lambda_c$, where λ_c is the wavelength at the cutoff frequency f_c . But, as shown in Fig. 2(c), a PSF that lacks a low frequency component does not concentrate in the center beam anymore, and the side beams of the PSF slowly attenuate as the position gets farther away from the point source, thereby introducing significant artifacts in the investigation of large objects.

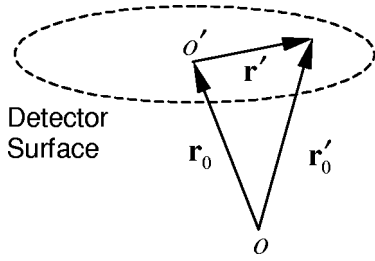


FIG. 3. Diagram of the detector surface \mathbf{r}' with origin o' . The vector \mathbf{r}_0 represents the center of detector o' in the recording geometry with origin o . The vector \mathbf{r}'_0 points to an element of the detector aperture.

In conclusion, the obtainable spatial resolution approximates to a value between $0.6\lambda_c$ and $0.8\lambda_c$, where λ_c is the wavelength at the high cutoff frequency f_c . If the bandwidth is too narrow, the reconstruction based on the wide bandwidth measurement becomes inappropriate and the FWHM of the reconstructed PSF does not properly describe the real spatial resolution.

IV. EFFECT OF DETECTOR APERTURE

Next, let us derive the analytic expressions of the PSF's related to detector aperture size. As shown in Fig. 3, the real signal detected at position \mathbf{r}_0 can be expressed as a surface integral over the detector aperture

$$\bar{p}'(\mathbf{r}_0, k) = \int \int \bar{p}(\mathbf{r}'_0, k) W(\mathbf{r}'_0) d^2\mathbf{r}'_0, \quad (57)$$

where $W(\mathbf{r}'_0)$ is a weighting factor, which represents the contribution from different elements of the detector surface to the total signal of the detector.

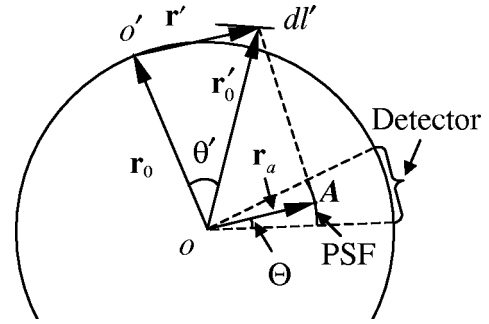
Since $\mathbf{r}'_0 = \mathbf{r}_0 + \mathbf{r}'$, Eq. (57) can be rewritten as

$$\bar{p}'(\mathbf{r}_0, k) = \int \int \bar{p}(\mathbf{r}_0 + \mathbf{r}', k) W(\mathbf{r}') d^2\mathbf{r}'. \quad (58)$$

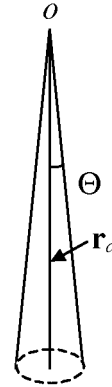
One can assume a point source at \mathbf{r}_a and then get the detected signal at position \mathbf{r}_0 using Eq. (57) or (58). If the signal is not bandlimited, by substituting $\bar{p}'(\mathbf{r}_0, k)$ for $p(\mathbf{r}_0, k)$ in the rigorous reconstruction formulas such as Eqs. (8)–(10), one can get analytic expressions of the PSF's for the spherical, planar, and cylindrical geometries, respectively. In general, the analytic expressions cannot be thoroughly simplified for arbitrary detector apertures. In order to explicitly demonstrate the effects of the detector apertures on spatial resolution, we will make some assumptions about the detector apertures.

A. Spherical geometry

As shown in Fig. 4(a), \mathbf{r}_0 represents the center of detector o' in the global spherical coordinates (r, θ, φ) with the origin at the recording geometry center o . A local spherical coordinate system aligned with \mathbf{r}_0 is used as well. Assume that the detector is circularly symmetric about its center o' ; in this case, the weighting factor depends only on θ' , $W(\mathbf{r}')$



(a)



(b)

FIG. 4. (a) Diagram of the spherical recording geometry: θ' is the angle between \mathbf{r}_0 and \mathbf{r}'_0 ; dl' is an integral element on the detector surface; Θ is the angle of the radius of the detector aperture to the recording geometry origin o ; the extension of the PSF at point A is indicated; other denotations of the symbols are the same as in Figs. 1 and 3. (b) Perspective view of the lateral extension of the PSF's of all the point sources along a radial axis in the spherical recording geometry.

$= W(\theta')$, where the angle θ' between \mathbf{r}'_0 and \mathbf{r}_0 —the polar angle of \mathbf{r}'_0 in the local coordinate system—varies from 0 to Θ depending on the size of the detector. The azimuthal angle φ' of \mathbf{r}'_0 in the local coordinate system varies from 0 to 2π . The normal of the detector surface at point o' is assumed to point to the center of the recording geometry o . The surface integral in Eq. (58) can be transformed into an integral over a curve radiating from the center o' on the surface l' and the azimuthal angle φ' :

$$\begin{aligned} \bar{p}'(\mathbf{r}_0, k) &= \int \int \bar{p}(\mathbf{r}_0 + \mathbf{r}', k) W(\theta') r' \sqrt{1 - (\mathbf{n}_0 \cdot \mathbf{n}')^2} d\varphi' dl' \\ &= \int_{l'} W(\theta') \sqrt{1 - (\mathbf{n}_0 \cdot \mathbf{n}')^2} r' dl' \\ &\quad \times \int_0^{2\pi} \bar{p}(\mathbf{r}_0 + \mathbf{r}', k) d\varphi', \end{aligned} \quad (59)$$

where $\mathbf{n}' = \mathbf{r}'/r'$ and

$$\tilde{p}(\mathbf{r}_0 + \mathbf{r}', k) = -ikc^2 \eta \frac{\exp(ik|\mathbf{r}_a - \mathbf{r}_0 - \mathbf{r}'|)}{4\pi|\mathbf{r}_a - \mathbf{r}_0 - \mathbf{r}'|}. \quad (60)$$

Considering the expansion in the local spherical coordinates, and denoting $\mathbf{n}'_0 = \mathbf{r}'_0/r'_0$, $\mathbf{n}'_0 = (\theta', \varphi')$, and $\mathbf{n}_a = (\theta'_a, \varphi'_a)$, one obtains

$$\frac{\exp(ik|\mathbf{r}_a - \mathbf{r}'_0|)}{4\pi|\mathbf{r}_a - \mathbf{r}'_0|} = \frac{ik}{4\pi} \sum_{l=0}^{\infty} (2l+1)j_l(kr_a) \times h_l^{(1)}(kr'_0)P_l(\mathbf{n}_a \cdot \mathbf{n}'_0), \quad (61)$$

where $P_l(\mathbf{n}_a \cdot \mathbf{n}'_0)$ can be expanded as [14]

$$P_l(\mathbf{n}_a \cdot \mathbf{n}'_0) = P_l(\cos \theta'_a)P_l(\cos \theta') + 2 \sum_{m=1}^l \frac{(l-m)!}{(l+m)!} P_l^m(\cos \theta'_a)P_l^m(\cos \theta') \times \cos[m(\varphi'_a - \varphi')]. \quad (62)$$

Then, one can evaluate the following integral:

$$\int_0^{2\pi} P_l(\mathbf{n}_a \cdot \mathbf{n}'_0) d\varphi' = 2\pi P_l(\cos \theta')P_l(\cos \theta'_a). \quad (63)$$

Actually, θ'_a is the angle between \mathbf{r}_0 and \mathbf{r}_a , i.e., $\cos \theta'_a = \mathbf{n}_a \cdot \mathbf{n}_0$.

Combining the results of Eqs. (61)–(63), Eq. (59) can be rewritten as

$$\begin{aligned} \tilde{p}'(\mathbf{r}_0, k) &= \frac{k^2 c^2 \eta}{2} \int_{l'} W(\theta') \sqrt{1 - (\mathbf{n}_0 \cdot \mathbf{n}')^2} r' dl' \\ &\times \sum_{l=0}^{\infty} (2l+1) P_l(\cos \theta') P_l(\mathbf{n}_a \cdot \mathbf{n}_0) j_l(kr_a) \\ &\times h_l^{(1)}(kr'_0). \end{aligned} \quad (64)$$

By replacing $p(\mathbf{r}_0, k)$ with $\tilde{p}'(\mathbf{r}_0, k)$ in the reconstruction formula Eq. (8) and considering identity (14), one obtains the reconstruction for $A(\mathbf{r})$:

$$\begin{aligned} A_a(\mathbf{r}) &= \frac{1}{\pi} \int_{l'} W(\theta') \sqrt{1 - (\mathbf{n}_0 \cdot \mathbf{n}')^2} r' dl' \\ &\times \sum_{m=0}^{\infty} (2m+1) P_m(\mathbf{n}_a \cdot \mathbf{n}) P_m(\cos \theta') \\ &\times \int_0^{+\infty} j_m(kr_a) j_m(kr) \frac{h_m^{(1)}(kr'_0)}{h_m^{(1)}(kr_0)} k^2 dk. \end{aligned} \quad (65)$$

Letting $\tilde{\theta}$ and $\tilde{\varphi}$ be the polar and azimuthal angles of vector \mathbf{n} with respect to vector \mathbf{n}_a , and using an identity similar to the one shown in Eq. (63), one can rewrite Eq. (65) as

$$\begin{aligned} A_a(\mathbf{r}) &= \int \int W(\theta') r' \sqrt{1 - (\mathbf{n}_0 \cdot \mathbf{n}')^2} d\varphi' dl' \\ &\times \frac{1}{2\pi^2} \sum_{m=0}^{\infty} (2m+1) P_m(\cos \tilde{\gamma}) \\ &\times \int_0^{+\infty} j_m(kr_a) j_m(kr) \frac{h_m^{(1)}(kr'_0)}{h_m^{(1)}(kr_0)} k^2 dk, \end{aligned} \quad (66)$$

where $\cos \tilde{\gamma} = \cos \tilde{\theta} \cos \theta' + \sin \tilde{\theta} \sin \theta' \cos(\tilde{\varphi} - \varphi')$.

1. Special spherical aperture

For simplicity, assume that the detector is a small section of the spherical measurement surface, i.e., $r'_0 = |\mathbf{r}'_0| = |\mathbf{r}_0 + \mathbf{r}'| = |\mathbf{r}_0| = r_0$. Therefore, one obtains

$$\sqrt{1 - (\mathbf{n}_0 \cdot \mathbf{n}')^2} r' dl' = r_0^2 \sin \theta' d\theta', \quad (67)$$

and

$$h_m^{(1)}(kr'_0)/h_m^{(1)}(kr_0) = 1. \quad (68)$$

Substituting the identity Eq. (18) and the following identity (see the Appendix) into Eq. (65),

$$\sum_{m=0}^{\infty} (2m+1) P_m(\mathbf{n}_a \cdot \mathbf{n}) P_m(\cos \theta') = 2 \delta(\cos \theta' - \mathbf{n}_a \cdot \mathbf{n}), \quad (69)$$

one obtains

$$A_a(\mathbf{r}) = \frac{r_0^2}{r^2} \delta(r - r_a) \int_0^{\Theta} \sin \theta' W(\theta') d\theta' \delta(\cos \theta' - \mathbf{n}_a \cdot \mathbf{n}). \quad (70)$$

Letting γ be the angle between \mathbf{n}_a and \mathbf{n} , i.e., $\mathbf{n}_a \cdot \mathbf{n} = \cos \gamma$,

$$\begin{aligned} A_a(\mathbf{r}) &= \frac{r_0^2}{r^2} \delta(r - r_a) \int_0^{\Theta} \sin \theta' W(\theta') d\theta' \delta(\cos \theta' - \cos \gamma) \\ &= \frac{r_0^2}{r^2} \delta(r - r_a) \int_0^{\Theta} \sin \theta' W(\theta') d\theta' \frac{\delta(\theta' - \gamma)}{\sin \theta'} \\ &= \frac{r_0^2}{r^2} \delta(r - r_a) \int_0^{\Theta} W(\theta') \delta(\theta' - \gamma) \delta\theta' \\ &= \frac{r_0^2}{r^2} \delta(r - r_a) W(\gamma). \end{aligned} \quad (71)$$

If letting $W(\theta') = 1$,

$$A_a(\mathbf{r}) = \frac{r_0^2}{r^2} \delta(r - r_a) [U(\gamma) - U(\gamma - \Theta)], \quad (72)$$

where U is the step function, $U(x) = 1$ when $x > 0$ and $U(x) = 0$ when $x < 0$.

Equation (72) indicates that, in this special case, the PSF only extends along the lateral direction, which is proportional to the solid angle of the detector aperture to the origin

of the measurement geometry. The perspective view of the lateral extension of all the points in a radial axis looks like a cone as shown in Fig. 4(b). The farther the point source is away from the origin, the more extension the PSF has. Therefore, the lateral resolution is worse when the point is close to the detector. But, a lateral resolution superior to the aperture size can still be achieved if the object under study is close to the center of the geometry.

2. Small flat aperture

Now, let us consider flat apertures. Sometimes, a set of small flat detectors is used to form a spherical recording surface. Suppose the detector aperture is disklike and its radius is P . Since $\mathbf{n}_0 \cdot \mathbf{n}' = 0$ in this case,

$$\sqrt{1 - (\mathbf{n}_0 \cdot \mathbf{n}')^2} r' dl' = r' dr', \quad (73)$$

where $r' = r_0 \tan \theta'$. If the aperture is small relative to the radius of the detection surface, i.e., $r' \leq P \ll r_0$, the following approximation holds:

$$r'_0 - r_0 = \sqrt{r_0^2 + r'^2} - r_0 \approx \frac{r'^2}{2r_0}. \quad (74)$$

Neglecting the second-order and higher small quantities, one can approximate $h_m^{(1)}(kr'_0)/h_m^{(1)}(kr_0) \approx 1$. Then, one can follow the derivation for the special spherical aperture and obtain

$$A_a(\mathbf{r}) = \frac{1}{r^2} \delta(r - r_a) \int_0^P W(r') r' dr' \delta(\cos \theta' - \mathbf{n}_a \cdot \mathbf{n}). \quad (75)$$

Letting $W(r') = 1$ and approximating $r' = r_0 \tan \theta' \approx r_0 \theta'$ for the small-aperture case, one reaches

$$\begin{aligned} A_a(\mathbf{r}) &\approx \frac{r_0^2}{r^2} \delta(r - r_a) \int_0^{P/r_0} \theta' \frac{\delta(\theta' - \gamma)}{\sin \theta'} d\theta' \\ &= \frac{r_0^2}{r^2} \delta(r - r_a) \int_0^{P/r_0} \delta(\theta' - \gamma) \delta\theta' \\ &= \frac{r_0^2}{r^2} \delta(r - r_a) [U(\gamma) - U(\gamma - P/r_0)]. \end{aligned} \quad (76)$$

Equation (76) indicates that, for the small flat aperture, the extension of the PSF is primarily along the lateral axis. In fact, if we substitute Θ for P/r_0 , Eq. (76) becomes identical to Eq. (72) for the special spherical aperture.

Particularly, at the center of the recording geometry, i.e., $r_a = 0$, we have $j_m(0) = \delta_{m0}$, $P_0(\cdot) = 1$, and $h_0^{(1)}(kr) = -i \exp(ikr)/(kr)$. Assuming $W(r') = 1$, Eq. (65) reduces to

$$\begin{aligned} A_a(\mathbf{r}) &= \frac{1}{\pi} \int_0^{+\infty} j_0(kr) \exp(-ikr_0) k^2 dk \\ &\times \int_0^P \frac{r_0}{r'_0} r' dr' \exp(ikr'_0). \end{aligned} \quad (77)$$

Using the relation $r'_0 = \sqrt{r_0^2 + r'^2}$, one can simplify Eq. (77) to

$$A_a(\mathbf{r}) = \frac{1}{\pi} \int_0^{+\infty} j_0(kr) k^2 dk \frac{r_0 [\exp(ik\sqrt{P^2 + r_0^2} - ikr_0) - 1]}{ik}. \quad (78)$$

Because $P \ll r_0$, the imaginary part is much less than the real part and hence can be neglected; as a result, one can obtain

$$A_a(\mathbf{r}) \approx \frac{r_0}{\pi} \int_0^{+\infty} j_0(kr) \sin[k(\sqrt{P^2 + r_0^2} - r_0)] k dk. \quad (79)$$

Using the following identity [14]:

$$\begin{aligned} \int_0^{+\infty} j_0(ka) \sin(kb) k dk &= b \int_0^{+\infty} j_0(ka) j_0(kb) k^2 dk \\ &= \frac{\pi}{2b} \delta(b - a), \end{aligned} \quad (80)$$

in the small-aperture case, i.e., $P \ll r_0$, Eq. (79) reduces to

$$A_a(r) = \frac{r_0^2}{P^2} \delta\left(r - \frac{P^2}{2r_0}\right). \quad (81)$$

Equation (79) indicates that the point source at the center becomes a circle with a diameter P^2/r_0 .

Next, we want to estimate the lateral extension at an arbitrary point. Taking the asymptotic form of the Hankel function to approximate

$$\frac{h_m^{(1)}(kr'_0)}{h_m^{(1)}(kr_0)} \approx \frac{\exp(ikr'_0)/(kr'_0)}{\exp(ikr_0)/(kr_0)} = \frac{r_0}{r'_0} \exp(ikr'_0 - ikr_0), \quad (82)$$

one can rewrite Eq. (65) as

$$\begin{aligned} A_a(\mathbf{r}) &= \frac{1}{\pi} \int_0^P W(r') r' dr' \int_0^{+\infty} \frac{r_0}{r'_0} \exp(ikr'_0 - ikr_0) k^2 dk \\ &\times \sum_{m=0}^{\infty} (2m+1) P_m(\mathbf{n}_a \cdot \mathbf{n}) \\ &\times P_m(\cos \theta') j_m(kr_a) j_m(kr). \end{aligned} \quad (83)$$

The above integral is still complicated. Here, we consider only the spread along \mathbf{r}_a with the assumption of $W(r') = 1$. Substituting $P_m(\mathbf{n}_a \cdot \mathbf{n}) = P_m(1) = 1$ into Eq. (83) and considering identity (16), and further approximating $j_0(k\sqrt{r_a^2 + r^2 - 2r_a r \cos \theta'}) \approx j_0(k|r - r_a|)$ for the small-aperture case ($r' \ll r_0$, i.e., $\theta' \ll 1$), one obtains

$$\begin{aligned} A_a(r\mathbf{n}_a) &= \frac{1}{\pi} \int_0^{+\infty} j_0(k|r - r_a|) \exp(-ikr_0) k^2 dk \\ &\times \int_0^P \frac{r_0}{r'_0} r' dr' \exp(ikr'_0). \end{aligned} \quad (84)$$

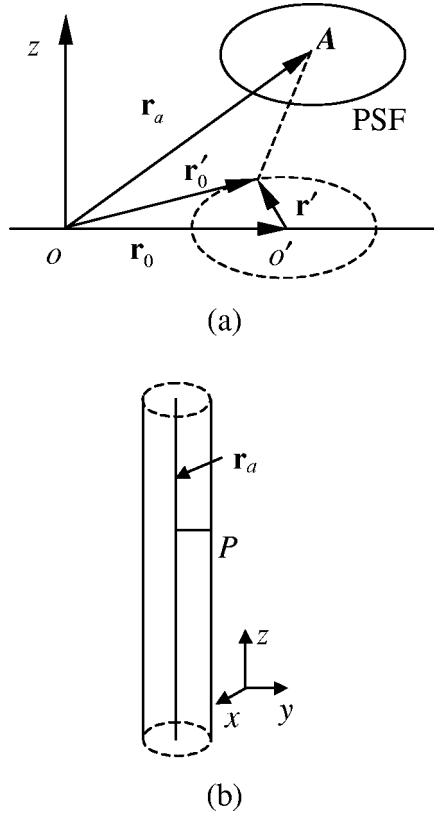


FIG. 5. (a) Diagram of the planar recording geometry: P is the radius of the detector aperture; the extension of the PSF at point A is indicated; other denotations of the symbols are the same as in Figs. 1 and 3; (b) perspective view of the lateral extension of the PSF's of all the point sources along a line parallel to the z axis in the planar recording geometry.

If we substitute $|r - r_a|$ for r , Eq. (84) becomes identical to Eq. (77). Thus, in the small-aperture case ($P \ll r_0$), Eq. (84) reduces to Eq. (81) with the replacement of r by $|r - r_a|$:

$$A_a(r\mathbf{n}_a) \approx \frac{r_0^2}{P^2} \delta\left(|r - r_a| - \frac{P^2}{2r_0}\right). \quad (85)$$

Equation (85) indicates that the point source at which \mathbf{r}_a extends in the radial direction to a region with diameter P^2/r_0 is the same as the extension of the PSF at the recording geometry center as shown in Eq. (81). But, in most cases, this extension is negligible. For example, when using a transducer with even a 6 mm diameter to image a 10-cm-size breast on a recording geometry surface with a 15 cm diameter, $P^2/r_0 = 3^2/150 = 0.06$ mm. However, the lateral extension at r is on the order of $2rP/r_0$ as shown in Eq. (76). For example, even at $r = 1$ cm, $2rP/r_0 = (2)(10)(3)/150 = 0.4$ mm > 0.06 mm.

B. Planar geometry

In this case, we reasonably assume that the detector surface is flat. As shown in Fig. 5(a), \mathbf{r}_0 represents the center of the detector o' in the global Cartesian coordinates (x, y, z) with the origin at the recording geometry center o . Let x' ,

y' , and z' be the differences of the coordinates between \mathbf{r}'_0 and \mathbf{r}_0 , respectively. For the following two linear translations:

$$\mathbf{r}_0 \rightarrow \mathbf{r}'_0: x_0 \rightarrow x_0 + x' = x'_0, \quad y_0 \rightarrow y_0 + y' = y'_0, \quad (86)$$

$$\mathbf{r}_a \rightarrow \mathbf{r}'_a: x_a \rightarrow x_a - x' = x'_a, \quad y_a \rightarrow y_a - y' = y'_a, \quad (87)$$

there exist the following translational invariances, $|\mathbf{r}_a - \mathbf{r}'_0| = |\mathbf{r}'_a - \mathbf{r}_0|$.

The detected signal at \mathbf{r}_0 can be written as

$$\begin{aligned} \bar{p}'(\mathbf{r}_0, k) &= \int \int W(\mathbf{r}') \bar{p}(\mathbf{r}_0 + \mathbf{r}', k) d^2\mathbf{r}' \\ &= \int \int W(x', y') \bar{p}(x_0 + x', y_0 + y', k) dx' dy'. \end{aligned} \quad (88)$$

Using $\bar{p}'(\mathbf{r}_0, k)$ to replace $p(\mathbf{r}_0, k)$ in the reconstruction formula Eq. (9), and following the similar derivation shown in Sec. III B, one gets the reconstruction for $A(\mathbf{r})$ as

$$\begin{aligned} A_a(x, y, z) &= \int \int W(x', y') \delta(x - x'_a) \delta(y - y'_a) \\ &\quad \times \delta(z - z_a) dx' dy' \\ &= \int \int W(x', y') \delta(x - x_a + x') \delta(y - y_a + y') \\ &\quad \times \delta(z - z_a) dx' dy', \end{aligned} \quad (89)$$

i.e.,

$$A_a(x, y, z) = W(x - x_a, y - y_a) \delta(z - z_a). \quad (90)$$

Assuming that the detector surface is a disk with radius P , and $W(x', y') = 1$ when $\sqrt{x'^2 + y'^2} < P$, Eq. (90) reduces to

$$A_a(x, y, z) = U(P - D) \delta(\Delta z), \quad (91)$$

where $D = \sqrt{(\Delta x)^2 + (\Delta y)^2}$, and $\Delta x = x - x_a$, etc.

Equation (91) indicates that without considering the bandwidth, the PSF does not extend along the axial direction, but it greatly extends in the lateral direction. Moreover, the lateral extension is proportional to the detector aperture. The perspective view of the lateral extension of all the PSF's in a line parallel with the z axis looks like a cylinder as shown in Fig. 5(b). Therefore, the lateral resolution is totally blurred by the detector aperture, no matter where the point is.

C. Cylindrical geometry

1. Special cylinder aperture

We first assume that the detector surface is a section of the cylindrical measurement surface. As shown in Fig. 6(a), \mathbf{r}_0 represents the center of the detector o' in the global cylindrical coordinates (ρ, φ, z) with the origin at the recording geometry center o . Let φ' be the difference between the polar angles of \mathbf{r}_0 and \mathbf{r}'_0 , and ρ' and z' be the projections of

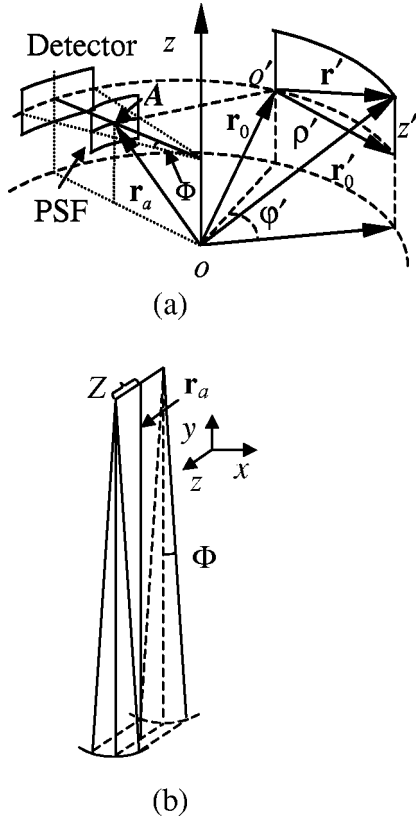


FIG. 6. (a) Diagram of the cylindrical geometry: φ' is the difference between the polar angles of \mathbf{r}_0 and \mathbf{r}'_0 ; ρ' and z' are the projections of \mathbf{r}' in the x - y plane and the z axis, respectively; Z is the half width of the detector aperture along the z axis and Φ is the half angle of the width of the detector aperture parallel to the x - y plane to the center of the recording geometry; the extension of the PSF at point A is indicated; other denotations of the symbols are the same as in Figs. 1 and 3. (b) Perspective view of the lateral extension of the PSF's of all the point sources along a radial axis in the cylindrical recording geometry.

\mathbf{r}' in the x - y plane and the z axis, respectively. Two sides of the detector are along the z axis from $-Z$ to Z , and the other two sides are parallel with the x - y plane and the polar angle φ' varies from $-\Phi$ to Φ . For the following two translations:

$$\mathbf{r}_0 \rightarrow \mathbf{r}'_0: \quad \varphi_0 \rightarrow \varphi_0 + \varphi' = \varphi'_0, \quad z_0 \rightarrow z_0 + z' = z'_0, \quad (92)$$

$$\mathbf{r}_a \rightarrow \mathbf{r}'_a: \quad \varphi_a \rightarrow \varphi_a - \varphi' = \varphi'_a, \quad z_a \rightarrow z_a - z' = z'_a, \quad (93)$$

there exist the following translational invariances, $|\mathbf{r}_a - \mathbf{r}'_0| = |\mathbf{r}'_a - \mathbf{r}_0|$.

The detected signal can be written as

$$\begin{aligned} \bar{p}_a(\mathbf{r}_0, k) &= \int \int \bar{p}(\mathbf{r}_0 + \mathbf{r}', k) W(\mathbf{r}') d^2 \mathbf{r}' \\ &= \int \int \bar{p}(\varphi_0 + \varphi', z_0 + z', k) W(\varphi', z') \rho_0 d\varphi' dz'. \end{aligned} \quad (94)$$

Replacing $p(\mathbf{r}_0, k)$ by $\bar{p}'(\mathbf{r}_0, k)$ in the reconstruction formula Eq. (10), and following the derivation shown in Sec. III C, one can get the reconstruction for $A(\mathbf{r})$ as

$$\begin{aligned} A_a(\rho, \varphi, z) &= \int \int \frac{1}{\rho} \delta(\rho - \rho_a) \delta(\varphi - \varphi'_a) \\ &\quad \times \delta(z - z'_a) W(\varphi', z') \rho_0 d\varphi' dz' \\ &= \frac{\rho_0}{\rho} \delta(\rho - \rho_a) \int \int \delta(\varphi - \varphi_a + \varphi') \\ &\quad \times \delta(z - z_a + z') W(\varphi', z') d\varphi' dz', \end{aligned} \quad (95)$$

i.e.,

$$A_a(\rho, \varphi, z) = \frac{\rho_0}{\rho} \delta(\rho - \rho_a) W(\varphi - \varphi_a, z - z_a). \quad (96)$$

If $W(\varphi', z') = 1$, φ' from $-\Phi$ to Φ , and z' from $-Z$ to Z , Eq. (96) can be rewritten as

$$A_a(\rho, \varphi, z) = \frac{\rho_0}{\rho} \delta(\rho - \rho_a) U(\Phi - |\varphi - \varphi_a|) U(Z - |z - z_a|). \quad (97)$$

Equation (97) indicates that the extension of the PSF in the cylindrical geometry combines the properties of the PSF's in the spherical and planar geometries. In this special case, the PSF does not extend along the radial direction. The perspective view of the lateral extension of all the point sources in a radial axis looks like a wedge of pie as shown in Fig. 6(b). In the z -axis direction, the PSF extension is proportional to the detector size along the z axis, just like the planar geometry. While parallel with the x - y plane, the lateral extension is proportional to the angle of the detector width to the z axis, just like in the spherical case. Therefore, a lateral resolution that is better than the aperture size can be obtained parallel to the x - y plane if the object under study is close to the center of the geometry; however, the lateral resolution along the z axis is determined by the detector size.

2. Small rectangle aperture

Sometimes a set of small rectangle detectors is used to form a cylindrical array. The normal of the detector at the center point o' is assumed to point to the center of the recording geometry. Two sides of the detector are along the z axis from $-Z$ to Z , and the other two sides are parallel with the x - y plane and have a length of $2P$. One can follow the similar derivation in Sec. III C, and get the reconstruction for $A(\mathbf{r})$ as

$$\begin{aligned}
A_a(\rho, \varphi, z) &= \frac{1}{2\pi} \int_{-Z}^Z \delta(z_a - z - z') dz' \int_{-P}^P d\rho' W(\varphi', z') \\
&\times \sum_{m=-\infty}^{+\infty} \exp[im(\varphi_a - \varphi - \varphi')] \\
&\times \int_0^{+\infty} \mu d\mu \\
&\times J_m(\mu\rho_a) J_m(\mu\rho) \frac{H_m^{(1)}(\mu\sqrt{\rho_0^2 + \rho'^2})}{H_m^{(1)}(\mu\rho_0)}, \quad (98)
\end{aligned}$$

where $\rho' = \rho_0 \tan \varphi'$. Let $W(\varphi', z') = 1$.

For the small-aperture case, $\rho' \ll \rho_0$, one can approximate

$$\frac{H_m^{(1)}(\mu\sqrt{\rho_0^2 + \rho'^2})}{H_m^{(1)}(\mu\rho_0)} \approx 1. \quad (99)$$

Further, taking the small-aperture approximation $\rho' = \rho_0 \tan \varphi' \approx \rho_0 \varphi'$, and considering the following identity [14]:

$$\int_0^{+\infty} \mu d\mu J_m(\mu\rho_a) J_m(\mu\rho) = \frac{1}{\rho} \delta(\rho - \rho_a), \quad (100)$$

one can rewrite Eq. (98) as

$$\begin{aligned}
A_a(\rho, \varphi, z) &= U(Z - |z - z_a|) \frac{1}{\rho} \delta(\rho - \rho_a) \\
&\times \int_{-P/\rho_0}^{P/\rho_0} \rho_0 d\varphi' \delta(\varphi_a - \varphi - \varphi'), \quad (101)
\end{aligned}$$

i.e.,

$$A_a(\rho, \varphi, z) = \frac{\rho_0}{\rho} \delta(\rho - \rho_a) U\left(\frac{P}{\rho_0} - |\varphi - \varphi_a|\right) U(Z - |z - z_a|). \quad (102)$$

Equation (102) indicates that, for the small flat aperture, the extension of the PSF is primarily along the lateral axis. In fact, if we substitute Φ for P/ρ_0 , Eq. (102) becomes identical to Eq. (97) in the special cylinder aperture case.

Next, we want to estimate the lateral extension of the PSF. One can also take the asymptotic form of the Hankel function to approximate

$$\frac{H_m^{(1)}(\mu\sqrt{\rho_0^2 + \rho'^2})}{H_m^{(1)}(\mu\rho_0)} \approx \exp[i\mu(\sqrt{\rho_0^2 + \rho'^2} - \rho_0)], \quad (103)$$

and then rewrite Eq. (98) as

$$\begin{aligned}
A_a(\rho, \varphi, z) &= \frac{1}{2\pi} U(Z - |z - z_a|) \int_0^{+\infty} \mu d\mu \\
&\times \int_{-P}^P d\rho' \exp[i\mu(\sqrt{\rho_0^2 + \rho'^2} - \rho_0)] \\
&\times \sum_{m=-\infty}^{+\infty} J_m(\mu\rho_a) J_m(\mu\rho) \\
&\times \exp[im(\varphi_a - \varphi - \varphi')]. \quad (104)
\end{aligned}$$

Considering identity (35), Eq. (104) can be rewritten as

$$\begin{aligned}
A_a(\rho, \varphi, z) &= \frac{1}{2\pi} U(Z - |z - z_a|) \int_0^{+\infty} \mu d\mu \\
&\times \int_{-P}^P d\rho' \exp[i\mu(\sqrt{\rho_0^2 + \rho'^2} - \rho_0)] \\
&\times J_0(\mu\sqrt{\rho_a^2 + \rho^2 - 2\rho_a\rho \cos(\varphi_a - \varphi - \varphi')}). \quad (105)
\end{aligned}$$

Equation (105) is still complicated. Here, by only considering the points along \mathbf{r}_a , i.e., letting $\varphi = \varphi_a$, and then taking the small-aperture approximation ($\varphi' \ll 1$),

$$J_0(\mu\sqrt{\rho_a^2 + \rho^2 - 2\rho_a\rho \cos(\varphi_a - \varphi - \varphi')}) \approx J_0(\mu|\rho - \rho_a|), \quad (106)$$

and

$$\sqrt{\rho_0^2 + \rho'^2} - \rho_0 \approx \frac{\rho'^2}{2\rho_0}, \quad (107)$$

one can rewrite Eq. (105) as

$$\begin{aligned}
A_a(\rho, \varphi_a, z) &= U(Z - |z - z_a|) \int_{-P}^P d\rho' \int_0^{+\infty} \mu d\mu \\
&\times J_0(\mu|\rho - \rho_a|) \exp(i\mu\rho'^2/2\rho_0). \quad (108)
\end{aligned}$$

Because $\rho' \ll \rho_0$, the imaginary part is much less than the real part and hence can be neglected,

$$\begin{aligned}
A_a(\rho, \varphi_a, z) &= U(Z - |z - z_a|) \int_{-P}^P d\rho' \int_0^{+\infty} \mu d\mu \\
&\times J_0(\mu|\rho - \rho_a|) \cos(\mu\rho'^2/2\rho_0) \\
&= U(Z - |z - z_a|) \int_{-P}^P d\rho' \left(\frac{\rho_0}{\rho'}\right) \frac{\partial}{\partial \rho'} \\
&\times \int_0^{+\infty} d\mu J_0(\mu|\rho - \rho_a|) \sin(\mu\rho'^2/2\rho_0). \quad (109)
\end{aligned}$$

Using the following identity [15]:

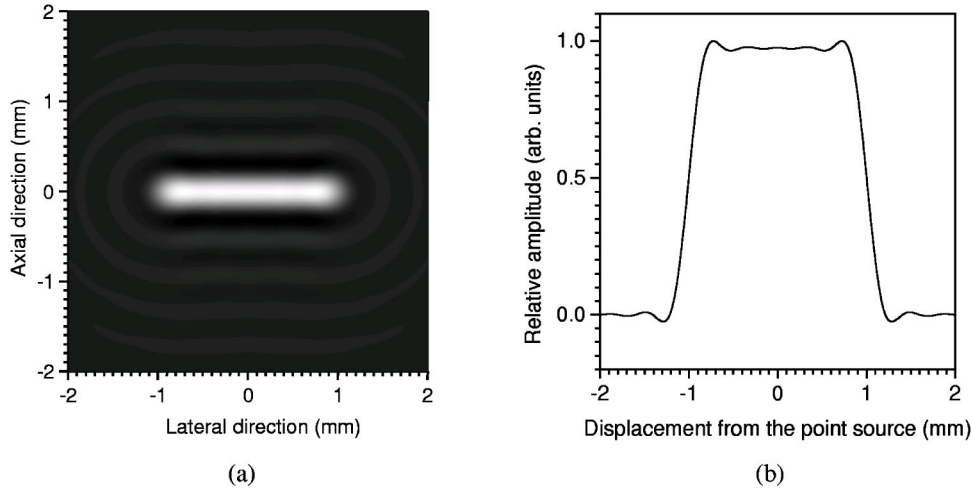


FIG. 7. An example of the PSF due to the detector aperture: (a) a gray scale view and (b) a lateral profile through the point source.

$$\int_0^{+\infty} dt J_0(ta) \sin(tb) = \begin{cases} \frac{1}{\sqrt{b^2 - a^2}}, & 0 < a < b \\ 0 & \text{otherwise,} \end{cases} \quad (110)$$

one can get the integral in Eq. (109),

$$\begin{aligned} & \int_{-P}^P d\rho' \left(\frac{\rho_0}{\rho'} \right) \frac{\partial}{\partial \rho'} \left[\sqrt{(\rho'^2/2\rho_0)^2 - |\rho - \rho_a|^2} \right]^{-1} \\ &= \left(\frac{\rho_0}{\rho'} \right) \left[\sqrt{(\rho'^2/2\rho_0)^2 - |\rho - \rho_a|^2} \right]^{-1} \Big|_{-P}^P \\ & \quad - \int_{-P}^P \left[\sqrt{(\rho'^2/2\rho_0)^2 - |\rho - \rho_a|^2} \right]^{-1} d \left(\frac{\rho_0}{\rho'} \right). \end{aligned} \quad (111)$$

The integral of Eq. (111) only exists in the range $P^2/2\rho_0 > |\rho - \rho_a|$. Therefore, the PSF extends to a region with a diameter P^2/ρ_0 , which is negligible compared to the lateral extension as we discussed in the spherical geometry explanation.

So far, we have derived the analytic PSF's due to the detector apertures for the specific spherical, planar, and cylindrical recording geometries. The explicit expressions can be given when the detector surfaces are assumed to have the same geometric properties as the recording geometries. Otherwise, it appears that explicitly carrying out the analytic derivations is impossible. But, in reality, the detector aperture is very small compared to the recording surface. We have also estimated axial extension in this case and found that it was negligible compared to lateral extension.

V. DISCUSSION AND CONCLUSIONS

In Sec. III, we proved that the PSF as a function of bandwidth is space invariant. In Sec. IV, we demonstrated that the finite aperture of the detector extends the PSF for different recording geometries.

Finally, we attempt to analyze the combined effects of bandwidth and detector size together. Assume that the detected signal is bandlimited, characterized by $\tilde{H}(k)$ with a cutoff frequency k_c , and the detectors have the same geometries as the recording surfaces. One can then follow the derivations in Secs. III and IV and reach the following results.

(1) Spherical geometry:

$$A_{ba}(\mathbf{r}) = \int \int W(\theta') \mathcal{F}_b^{\text{PSF}}(R') r_0^2 \sin \theta' d\theta' d\varphi', \quad (112)$$

where $R' = \sqrt{r^2 + r_a^2 - 2rr_a \cos \tilde{\gamma}}$, $\cos \tilde{\gamma} = \cos \tilde{\theta} \cos \theta' + \sin \tilde{\theta} \sin \theta' \cos(\tilde{\varphi} - \varphi')$, and $\tilde{\theta}$ and $\tilde{\varphi}$ are the polar and azimuthal angles of vector \mathbf{n} with respect to vector \mathbf{n}_a , respectively.

(2) Planar geometry:

$$A_{ba}(x, y, z) = \int \int W(x', y') \mathcal{F}_b^{\text{PSF}}(R') dx' dy', \quad (113)$$

where $R' = \sqrt{(x - x_a + x')^2 + (y - y_a + y')^2 + (z - z_a)^2}$.

(3) Cylindrical geometry:

$$A_{ba}(\rho, \varphi, z) = \int \int W(\varphi', z') \mathcal{F}_b^{\text{PSF}}(R') \rho_0 d\varphi' dz', \quad (114)$$

where $R' = \sqrt{\rho^2 + \rho_a^2 - 2\rho\rho_a \cos(\varphi - \varphi_a + \varphi') + (z - z_a + z')^2}$.

Equations (112)–(114) clearly reveal that the PSF can be regarded as a convolution of the detector aperture with the space invariant $\mathcal{F}_b^{\text{PSF}}$. However, in the spherical geometry case, the convolution becomes complicated as shown in Eq. (112). Further, we can imagine how complicated the convolution could be with an arbitrary recording geometry using arbitrary-aperture detectors.

Let us take the PSF in the planar geometry case as an example, which is shown in Fig. 7. The detector aperture is assumed to be a disk with a radius of 1 mm and a cutoff frequency $f_c = 4$ MHz. In the axial direction, the extension of the PSF is similar to that shown in Fig. 2(b), which is deter-

mined by the bandwidth. However, as shown Fig. 7(b), the PSF greatly expands in the lateral direction, and its corresponding $\mathcal{W}_{\text{FWHM}} \approx 2$ mm, which is physically limited by the detector size.

In conclusion, spatial resolution as a function of bandwidth is space invariant for any recording geometry when the reconstruction is linear and exact. The bandwidth limits the obtainable spatial resolution. The detector aperture blurs lateral resolution greatly at different levels for different recording geometries but the effect on axial resolution is slight. The results offer clear instruction for designing appropriate thermoacoustic imaging systems with predefined spatial resolutions.

ACKNOWLEDGMENTS

This project was sponsored in part by the U.S. Army Medical Research and Materiel Command Grant No. DAMD17-00-1-0455, the National Institutes of Health Grant Nos. R21 EB00319-02 and R01 EB000712, the National Science Foundation Grant No. BES-9734491, and the Texas Higher Education Coordinating Board Grant No. ARP 000512-0063-2001.

APPENDIX

The completeness relation of the spherical harmonics $Y_{lm}(\theta, \varphi)$ [14,16] is

$$\begin{aligned} \sum_{l=0}^{\infty} \sum_{m=-l}^l Y_{lm}^*(\theta', \varphi') Y_{lm}(\theta, \varphi) \\ = \delta(\varphi - \varphi') \delta(\cos \theta - \cos \theta'), \end{aligned} \quad (\text{A1})$$

where

$$Y_{lm}(\theta, \varphi) = \sqrt{\frac{2l+1}{4\pi} \frac{(l-m)!}{(l+m)!}} P_l^m(\cos \theta) \exp(im\varphi). \quad (\text{A2})$$

Then, do an integral over φ from 0 to 2π of both sides of Eq. (A1),

$$\begin{aligned} \sum_{l=0}^{\infty} \sum_{m=-l}^l \frac{2l+1}{4\pi} \frac{(l-m)!}{(l+m)!} P_l^m(\cos \theta) P_l^m(\cos \theta') \\ \times \int_0^{2\pi} \exp[im(\varphi - \varphi')] d\varphi \\ = \sum_{l=0}^{\infty} \sum_{m=-l}^l \frac{2l+1}{4\pi} \frac{(l-m)!}{(l+m)!} P_l^m(\cos \theta) P_l^m(\cos \theta') 2\pi \delta_{m0} \\ = \sum_{l=0}^{\infty} \frac{2l+1}{4\pi} P_l(\cos \theta) P_l(\cos \theta') 2\pi \\ = \delta(\cos \theta - \cos \theta') \int_0^{2\pi} \delta(\varphi - \varphi') d\varphi = \delta(\cos \theta - \cos \theta'), \end{aligned} \quad (\text{A3})$$

i.e.,

$$\sum_{l=0}^{\infty} (2l+1) P_l(\cos \theta) P_l(\cos \theta') = 2\delta(\cos \theta - \cos \theta'). \quad (\text{A4})$$

-
- [1] C. G. A. Hoelen, F. F. M. de Mul, R. Pongers, and A. Dekker, *Opt. Lett.* **23**, 648 (1998).
- [2] R. A. Kruger, W. L. Kiser, K. D. Miller, H. E. Reynolds, D. R. Reinecke, G. A. Kruger, and P. J. Hofacker, *Proc. SPIE* **3916**, 150 (2000).
- [3] K. P. Köstli, D. Frauchiger, J. J. Niederhauser, G. Paltauf, H. P. Weber, and M. Frenz, *IEEE J. Sel. Top. Quantum Electron.* **7**, 918 (2001).
- [4] R. O. Esenaliev, A. A. Karabutov, and A. A. Oraevsky, *IEEE J. Sel. Top. Quantum Electron.* **5**, 981 (1999).
- [5] G. Ku and L.-H. V. Wang, *Med. Phys.* **28**, 4 (2001).
- [6] M. Xu, G. Ku, and L.-H. V. Wang, *Med. Phys.* **28**, 1958 (2001).
- [7] M. Xu and L.-H. V. Wang, *IEEE Trans. Med. Imaging* **21**, 814 (2002).
- [8] Y. Xu, D.-Z. Feng, and L.-H. V. Wang, *IEEE Trans. Med. Imaging* **21**, 823 (2002).
- [9] Y. Xu, M. Xu, and L.-H. V. Wang, *IEEE Trans. Med. Imaging* **21**, 829 (2002).
- [10] M. Xu and L.-H. V. Wang, *Med. Phys.* **29**, 1661 (2002).
- [11] M. Xu, Y. Xu, and L.-H. V. Wang, *IEEE Trans. Biomed. Eng.* (to be published).
- [12] Y. Xu and L.-H. V. Wang (unpublished).
- [13] A. C. Tam, *Rev. Mod. Phys.* **58**, 381 (1986).
- [14] G. B. Arfken and H. J. Weber, *Mathematical Methods for Physicists* (Academic, San Diego, 1995).
- [15] M. Abramowitz and I. A. Stegun, *Handbook of Mathematical Functions with Formulas, Graphs, and Mathematical Tables* (Dover, New York, 1965).
- [16] J. D. Jackson, *Classical Electrodynamics* (Wiley, New York, 1999).
- [17] P. M. Morse and K. U. Ingard, *Theoretical Acoustics* (McGraw-Hill, New York, 1968).